Available online at www.sciencedirect.com

jmr&t Journal of Materials Research and Technology

journal homepage: www.elsevier.com/locate/jmrt

Original Article

Identification and quantification of martensite in ferritic-austenitic stainless steels and welds

Amir Baghdadchi[*], *Vahid A. Hosseini*, *Leif Karlsson*

Department of Engineering Science, University West, Trollhättan, SE-461 86, Sweden

ARTICLE INFO

Article history:
Received 14 April 2021
Accepted 18 September 2021
Available online 7 October 2021

Keywords:
Duplex stainless steel
Mechanical polishing
Electrolytic polishing
Phase analysis
Martensite
Electron backscatter diffraction

ABSTRACT

This paper aims at the phase identification and quantification in transformation induced plasticity duplex stainless steel (TDSS) base and weld metal containing ferrite, austenite, and martensite. Light optical microscopy (LOM) and electron backscatter diffraction (EBSD) analysis were employed to analyze phases. Samples were either mechanically or electrolytically polished to study the effect of the preparation technique. Mechanical polishing produced up to 26% strain-induced martensite. Electrolytic polishing with 150 g citric acid, 300 g distilled water, 600 mL H_3PO_4, and 450 mL H_2SO_4 resulted in martensite free surfaces, providing high-quality samples for EBSD analysis. Martensite identification was challenging both with LOM, due to the similar etching response of ferrite and martensite, and with EBSD, due to the similar lattice structures of ferrite and martensite. An optimized Beraha color etching procedure was developed that etched martensite distinctively. A novel step-by-step EBSD methodology was also introduced considering grain size and orientation, which successfully identified and quantified martensite as well as ferrite and austenite in the studied TDSS. Although here applied to a TDSS, the presented EBSD methodology is general and can, in combination with knowledge of the metallurgy of the specific material and with suitable adaption, be applied to a multitude of multiphase materials. It is also general in the sense that it can be used for base material and weld metals as well as additive manufactured materials.

1. Introduction

Phase identification and quantification are important in multiphase materials since the proportions of phases influence properties. This is for example reflected in the behavior of duplex (ferritic-austenitic) stainless steel (DSS) where the best mechanical properties and corrosion resistance are usually achieved for approximately equal amounts of ferrite and austenite [1,2]. Welding and heat treatment, as important stages of fabrication, affect the ferrite and austenite balance in DSS [3]. Measurement of phase fractions is, therefore, required to assure that the manufactured part meets requirements [4,5]. Transformation induced plasticity (TRIP) duplex stainless steel (TDSS) is a newly developed DSS, in which the TRIP effect is employed to improve formability and strength [6,7]. The benefit of the TRIP effect is achieved by having a sufficient austenite fraction allowing deformation-

* Corresponding author.
E-mail address: amir.baghdadchi@hv.se (A. Baghdadchi).
https://doi.org/10.1016/j.jmrt.2021.09.153

induced martensitic transformation (DIMT) to occur during forming [2,8]. This is attained by adjusting the austenite (γ) stability via tuning proportions of alloying elements and controlling phase fractions, allowing subsequent austenite to martensite transformation [8,9]. Therefore, the measurement of phase fractions in TDSS subjected to processes such as welding, additive manufacturing, and heat treatment is of paramount importance.

Metastable austenite can transform to martensite during cutting, grinding, and mechanical polishing since the surface undergoes plastic deformation [10]. Metallography and measurement of phase fractions are therefore challenging for materials with metastable austenite. Rodelas et al. [11] compared mechanical polishing with electrolytic polishing for 304L stainless steel welds and found that mechanical polishing caused more than 11% martensite formation due to the deformation-induced during mechanical grinding and polishing. Pinto et al. [12] also observed austenite to martensite transformation during mechanical polishing of AISI 1520 and 1540 carbon steels and claimed that the retained austenite content is highly dependent on the final preparation method. Electrolytic polishing does not introduce any external stress or deformation into the surface and therefore has two main benefits compared to mechanical polishing [12]. Firstly, it prevents deformation-induced phase transformation. Secondly, it produces a stress-free and smooth surface well suited for electron backscatter diffraction (EBSD) analysis as the quality is influenced by lattice defects and surface topography [13].

In addition to the sample preparation, reliable data and image acquisition techniques can be challenging in multiphase materials, such as TDSS steels and welds, containing ferrite, austenite, and martensite. Light optical microscopy (LOM) may often successfully be used to identify and quantify different phases, but a proper etching method is the key to distinguish various phases.

Nital etching [14] or color etching using Beraha [15] have been applied to identify martensite in TRIP 690 and austenitic AISI 301 steels, respectively. Beraha can also differentiate ferrite and austenite in DSS [16]. However, the implementation of Beraha to contrast ferrite, austenite, and martensite can be difficult as ferrite and martensite are colored very similarly by this etchant. Hence, Beraha etching is not straightforward for distinguishing these three phases in TDSS.

A scanning electron microscope (SEM) equipped with an EBSD detector is well suited for the identification and quantification of ferrite with a body centered cubic (bcc) and austenite with a face centered cubic (fcc) structure [17]. In TDSS, the metastable austenite can transform into two types of martensite: (i) ε-martensite with a hexagonal close-packed (hcp) crystal structure, and (ii) α'-martensite with a body centered tetragonal (bct) crystal structure which is often called bcc-martensite [8,18–20]. However, in the presence of ferrite, EBSD identification of low carbon α'-martensite is problematic. This is due to the low degree of tetragonality of the martensite making the difference between the two lattice structures less than the EBSD indexing capability. Separation of ferrite and martensite with X-ray diffraction is also challenging, as the existence of martensite mainly broadens the ferrite diffraction peaks [21]. Magnetic measurement using for example FERITSCOPE is not practical for small welds and cannot be used to differentiate between the two magnetic phases; ferrite and martensite [22,23]. Therefore, the accurate measurement of phase fractions is challenging for structures containing a mixture of ferrite, austenite, and martensite.

The possibility of phase transformation of metastable austenite during sample preparation and the complexities of phase fraction measurement are two common obstacles in phase analysis of multiphase steels. This is, for instance as discussed above, the case for TDSS in which the contents of ferrite, austenite, and martensite play vital roles in determining corrosion and mechanical properties. The formation of martensite either during sample preparation or during fabrication processes such as welding, forming, and heat treatment as well as difficulties in distinguishing between ferrite and martensite make the phase analysis of TDSS troublesome. Therefore, in this study, a comprehensive comparison of LOM and EBSD analysis of samples prepared by mechanical and electrolytic polishing is presented to investigate the weaknesses and benefits of each method. Two methodologies capable of reliably identifying martensite in ferritic-austenitic microstructures are introduced, one using LOM and one using EBSD. It is illustrated that the LOM methodology can contrast the different phases in TDSS by fine-tuning the etching technique. However, the novel step-by-step EBSD methodology can successfully identify and quantify all phases, making it applicable to analyze the microstructure of multiphase steels containing martensite and ferrite.

2. Experimental

2.1. Material

Plates of FDX 27 (UNS S82031) TRIP DSS with the chemical composition presented in Table 1 and the thickness of 1.5 mm were used in this study. Two samples were used to investigate the effects of the sample preparation technique on phase analysis: base material (BM) and a sample firstly laser welded and then laser reheated (WR) to promote austenite fractions required for the application. The laser welding was performed with the laser power of 2700 W and the travel speed of 30 mm/s. The focal lengths of the collimating lens and focusing lens were 120 mm and 200 mm, respectively. In the laser reheating, the optics were similar to the welding, but the laser power and travel speed were 550 W and 9 mm/s, respectively. The welding was performed with a spot size of 1 mm on the plate

Table 1 – Chemical composition (wt.%) of FDX 27 TDSS.

	C	Si	Mn	P	S	Cr	Ni	Mo	Cu	N
FDX 27	0.03	0.42	1.09	0.024	0.001	20.0	2.8	1.20	0.33	0.186

surface. For the reheating pass, however, the focus was positioned 50 mm above the surface. The shielding gas was pure nitrogen in both laser welding and laser reheating. More details about welding and reheating procedures can be found in Ref. [24].

2.2. Sample preparation and etching

As illustrated in Fig. 1, both the BM and WR samples were prepared by first cutting and then grinding from 320# to 2500#. After that, the samples followed two different polishing routes: (i) mechanical polishing (MP) and (ii) electrolytic polishing (EP).

For mechanical polishing, 9 μm and 3 μm diamond suspensions were used followed by 0.05 μm alumina suspension polishing. The polishing time was 5 min for each step. The applied load and the diameter of mounting were 25 N and 30 mm, respectively. Two different samples with and without etching were produced to study the influence of polishing on the phase analysis with optical and scanning electron microscopy (SEM)-EBSD. Different combinations of Beraha reagent compositions and etching times were applied to investigate the effect of the etching procedure on martensite characterization:

a. 60 mL water, 30 mL HCl, 0.9 g potassium bisulfite for 8–10 s
b. 60 mL water, 30 mL HCl, 0.85 g potassium bisulfite for 10–12 s
c. 60 mL water, 30 mL HCl, 0.8 g potassium bisulfite for 12–15 s
d. 60 mL water, 30 mL HCl, 0.6 g potassium bisulfite for 10–12 s

In all experiments, the etching was done immediately (less than 10 s) after mechanical polishing to suppress oxide formation on the surface.

For electrolytic polishing or electropolishing, a set-up according to Fig. 2 was employed. An electrolyte solution consisting of 150 g citric acid, 300 g distilled water, 600 mL H_3PO_4, and 450 mL H_2SO_4 was used. This solution was selected as it is less hazardous than conventional EP solutions containing perchloric acid where there is a risk of explosion if not handled correctly [25,26]. The EP was performed for 25 s at a voltage and a current density of 15 V and 1 A/cm^2, respectively. To avoid pitting corrosion during EP, the electrolyte was cooled by an ice bath to allow polishing at around 0 °C. It was found beneficial to lightly shake the sample while polishing to ensure continuous refreshment of the solution at the sample surface.

2.3. Microstructure characterization

Microstructures were studied with both LOM and EBSD to investigate the effect of sample preparation methods.

A Zeiss Axio Imager.M2m optical microscope was used to study mechanically polished samples after etching and electrolytically polished samples as polished. Phase fraction measurements were performed by image analysis (IA) via the open-access ImageJ software. In IA the contents of each phase are estimated by pixel counting. The accuracy, therefore, depends on the etching procedure and the quality of LOM images. In this study, four images were investigated for each case to measure the average and standard deviation of phase fraction.

EBSD analysis of WR samples after mechanical and electrolytic polishing was performed with a ZEISS Gemini SEM 450 equipped with a Symmetry S2 EBSD detector from Oxford Instruments. The acceleration voltage, sample tilt angle, and

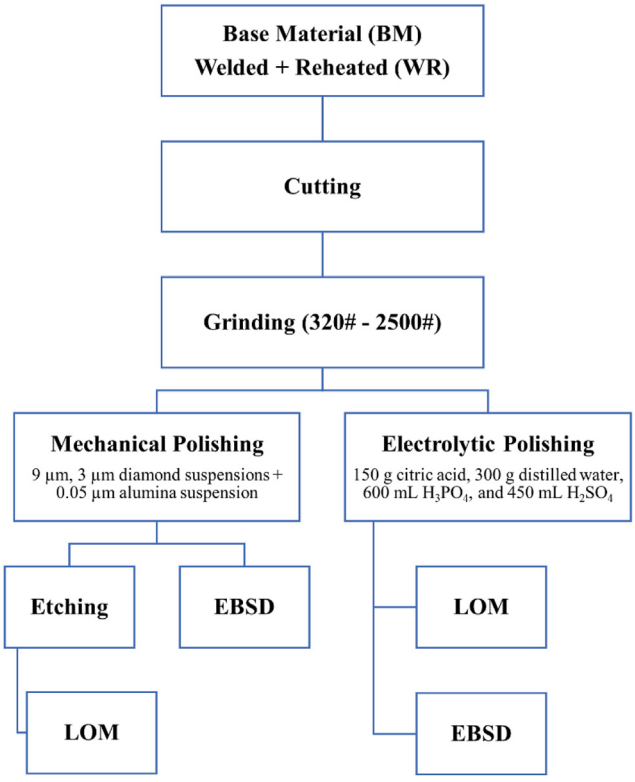

Fig. 1 – Sample preparation routes for light optical microscopy and electron backscatter diffraction analysis after mechanical or electrolytic polishing of BM and WR.

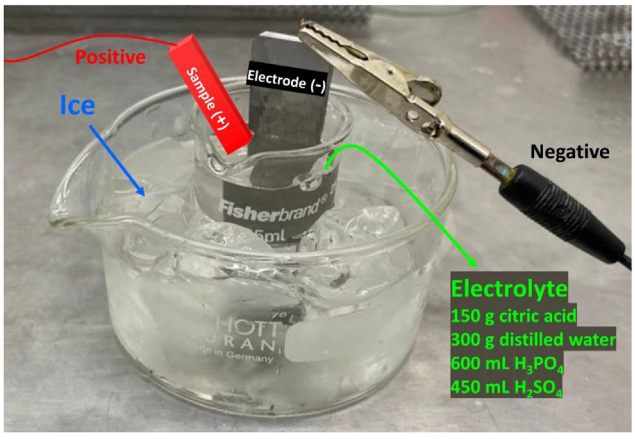

Fig. 2 – Electrolytic polishing procedure set-up. The counter electrode and the sample were negative and positive, respectively.

the working distance were 20 kV, 70°, and 10 mm, respectively. The AZtecCrystal 1.1 software from Oxford Instruments was used to analyze the EBSD results. EBSD mapping was performed with step sizes of 0.48 μm and 0.63 μm for mechanically and electrolytically polished samples, respectively.

3. Results

In this section, results of LOM and EBSD investigations of mechanically and electrolytically polished samples are presented. We, first, illustrate how the sample preparation method affects the martensite formation and how MP and EP can be used to prepare high-quality samples for phase characterization with LOM and EBSD. Then one LOM and one EBSD methodology are introduced for martensite identification as well as quantification.

3.1. *Influence of sample preparation*

3.1.1. *Light optical microscopy evaluation*

Low magnification cross-sections of the weld samples after mechanical or electrolytic polishing are illustrated in Fig. 3. As can be seen in Fig. 3-a, the bead geometry, ferrite (dark phase), and austenite (light phase) are visible after MP followed by color etching. However, Fig. 3-b demonstrates that EP is less suitable for LOM characterization of the weld zone or phases, at least at low magnification. This might be attributed to the inefficiency of color etching after electrolytic polishing.

Micrographs of wrought FDX 27 TDSS after mechanical or electrolytic polishing are shown in Fig. 4-a and -b, respectively. The microstructure after MP consists of ferrite, austenite, and martensite while the electropolished BM microstructure has only ferrite and austenite. It is noticeable that while MP together with etching resulted in a better contrast between phases, EP was also able to contrast ferrite and austenite enough to be quantifiable by IA. The mechanically and electrolytically polished samples contained 36 ± 4% and 37 ± 4% ferrite, respectively. The remaining was austenite for the EP sample, while the MP sample consisted of 38 ± 2% austenite and 26 ± 4% martensite.

Higher magnification micrographs of the laser welded and laser reheating FD×27 TDSS after MP and EP in Fig. 5 shows that, as for the BM, the mechanically polished sample, contained ferrite, austenite, and martensite while only ferrite and austenite could be observed after electrolytic polishing. The mechanically and electrolytically polished samples consisted of 44 ± 2% and 46 ± 5% ferrite, and 38 ± 2% and 54 ± 5% austenite, respectively. In addition, 18 ± 3% martensite was formed by mechanical polishing.

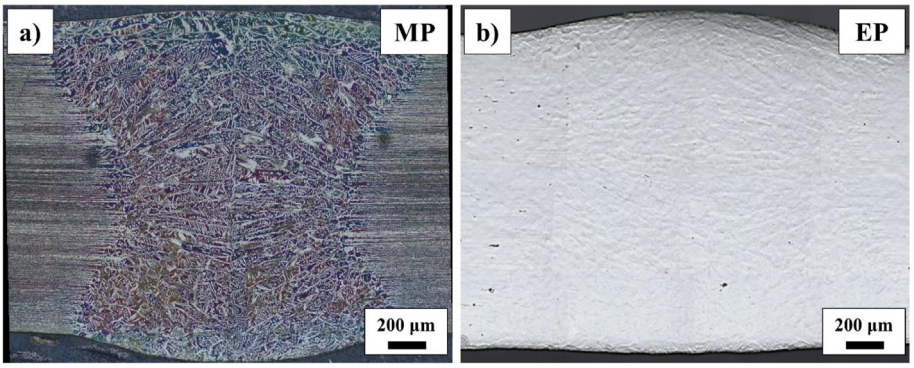

Fig. 3 – Cross-sections of laser welded and laser reheated FDX 27 TDSS a) after mechanical polishing and subsequent etching with Beraha and, b) after electrolytic polishing.

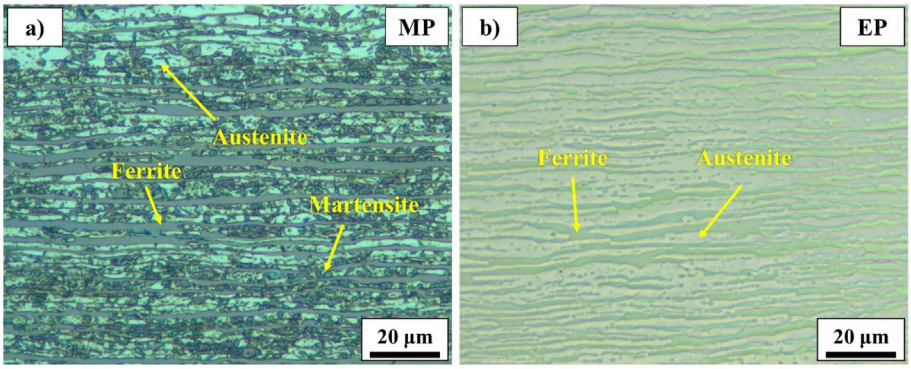

Fig. 4 – Light optical micrographs of FDX 27 TDSS. a) After mechanical polishing and etching with Beraha, showing ferrite, austenite, and martensite and, b) after electrolytic polishing with only ferrite and austenite.

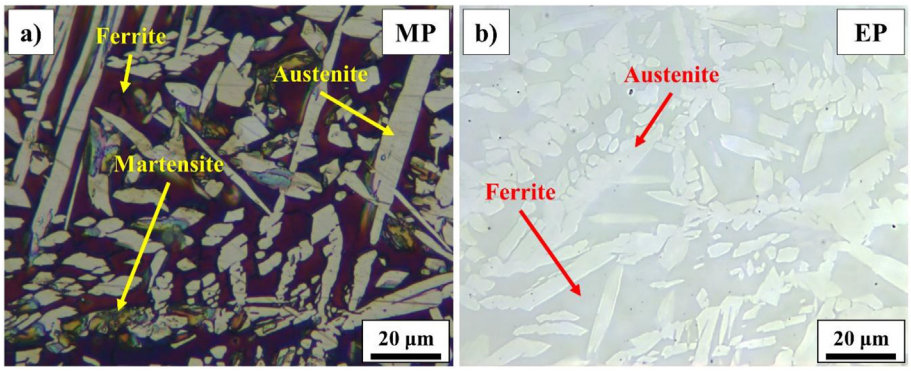

Fig. 5 – High magnification light optical micrographs of the WR sample, a) after mechanical polishing and subsequent etching with Beraha and, b) after electrolytic polishing.

3.1.2. *Electron backscatter diffraction evaluation*

In FDX 27 TDSS, austenite may transform to martensite due to the deformation [8] induced during the sample preparation. Band contrast (BC) maps from EBSD analysis of the TDSS welds after mechanical or electrolytic polishing are presented in Fig. 6. The blue arrows in the BC map shown in Fig. 6-a indicate that some scratches, or remaining below surface deformation, remained after mechanical polishing, which could affect the quality of EBSD analysis. On the other hand, electrolytic polishing as seen in Fig. 6-b produced a surface free from scratches and defects. The higher magnification BC maps in Fig. 6-c and -d demonstrate that although there were some strain patterns in the BC map of the mechanically polished sample, the electrolytic polishing made it possible to produce high-quality EBSD images suggesting a uniform and stress-free surface. The higher quality of BC images after EP is reflected in the capability of the EBSD analysis software in identifying the crystal structure, with 93.4% of points indexed for MP and 96.4% for EP.

The EBSD analysis of the WR samples after either mechanical or electrolytic polishing is shown in Fig. 7. The microstructures after MP or EP are presented as EBSD phase maps in Fig. 7-a and -b with bcc phase fractions of 69.1% for MP and 48.1% for EP samples. Inverse pole figures (IPF) of bcc after MP and EP are illustrated in Fig. 7-c and -d. A comparison of the MP and EP samples demonstrated that some small grains were indexed as bcc inside the austenite after mechanical polishing, while such grains could not be found in the electrolytically polished sample. The small bcc grains seen in Fig. 7-c had different orientations than the larger surrounding ferrite grain.

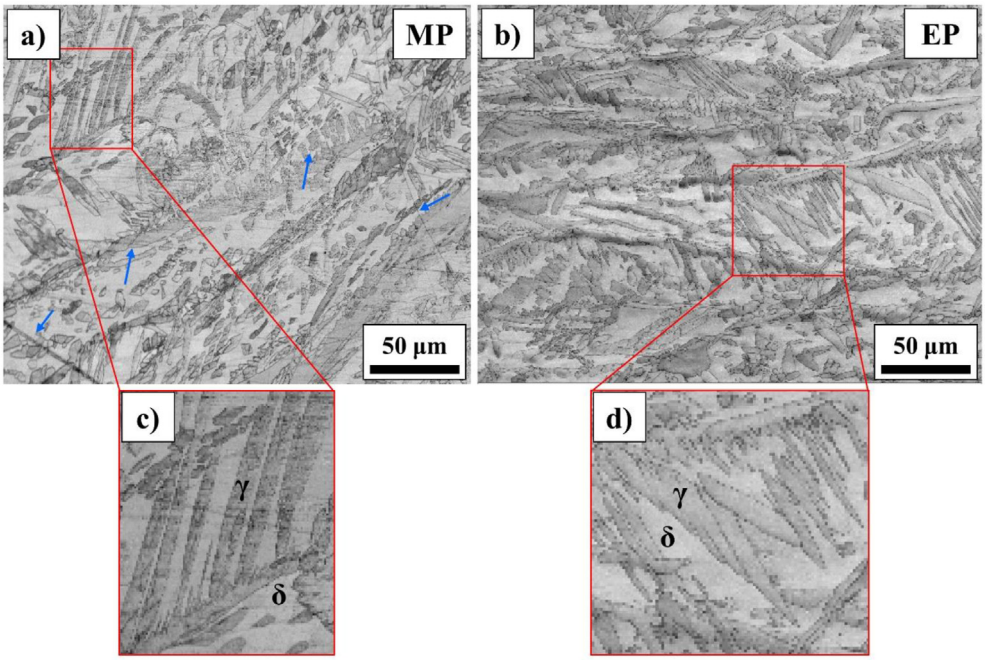

Fig. 6 – EBSD band contrast map of FDX 27 TDSS welds after a) mechanical polishing (unindexed points: 6.6%) containing scratches (blue arrows) and signs of surface deformation, and b) electrolytic polishing (unindexed points: 3.6%). c) patterns suggesting strain effects after mechanical polishing and, d) a high-quality BC map after electrolytic polishing.

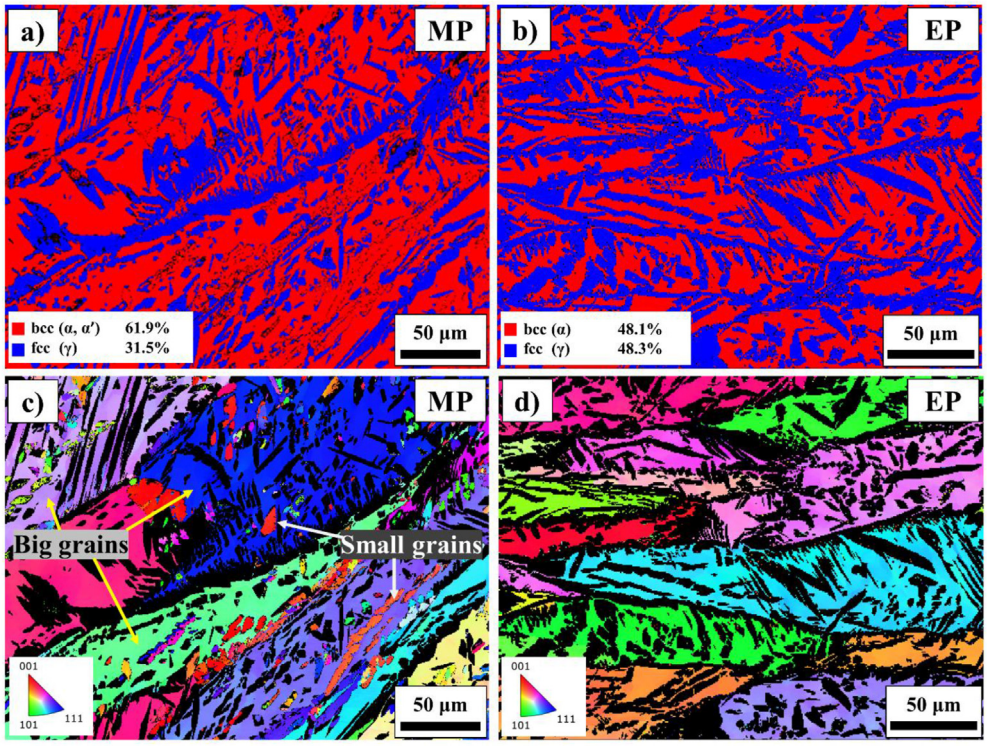

Fig. 7 – EBSD analysis after mechanical polishing (MP) and electrolytic polishing (EP) of FDX 27 TDSS welds. There was a significant difference between phase fractions indexed as bcc after MP and EP and small bcc grains inside austenite were only found after mechanical polishing. a, b) EBSD phase maps, and c, d) inverse pole figures (IPF) of bcc phase after MP and EP.

The big grains were therefore interpreted as ferrite and the small as martensite formed inside the austenite.

3.2. *Martensite identification and quantification methodologies*

Methodologies for identification and quantification of major phases, with a focus on martensite, in a TDSS weld are presented.

3.2.1. *Light optical microscopy*

Four micrographs from the same region of the mechanically polished WR sample after applying different Beraha etching procedures are shown in Fig. 8. It should be noted that although they are from the same location, they are from slightly different depths, as the sample was mechanically repolished to remove the effect of the previous etching. It was found that the etching procedure using a Beraha reagent with the composition of 60 mL water, 30 mL HCl, and 0.9 g potassium bisulfite for 8–10 s was not successful in distinguishing martensite and ferrite (Fig. 8-a). Changing the etchant composition to 60 mL water, 30 mL HCl, and 0.85 g potassium bisulfite and increasing etching time to 10–12 s improved the microstructure characterization with revealing the boundaries between martensite and ferrite or austenite. The color of martensite, however, was similar to that of ferrite, making IA unreliable (Fig. 8-b). Thereafter, decreasing the content of potassium bisulfite to 0.8 g and increasing etching time to 12–15 s, made martensite grains having a different color than ferrite and austenite. However, some grain boundaries and the surrounding areas were over-etched due to the relatively long etching time, resulting in poor accuracy of phase fraction measurement (Fig. 8-c). Finally, a Beraha reagent with the composition of 60 mL water, 30 mL HCl, and 0.6 g potassium bisulfite applied for 10–12 s produced an etched microstructure with clearly distinguishable colors of ferrite, austenite, and martensite, making IA possible (Fig. 8-d).

3.2.2. *Electron backscatter diffraction*

A novel EBSD methodology for phase identification and quantification of microstructures with both ferrite and martensite is introduced in Fig. 9. Differentiating between ferrite and low carbon bct-martensite phases is, as discussed earlier, difficult with EBSD. However, ferrite and martensite can in TDSS welds be separated based on their grain size and grain orientation. The methodology is explained using an EBSD phase map of a microstructure with ferrite, austenite, and martensite from the location studied by LOM in Fig. 8. The steps involved in the identification and separation of the martensite from ferrite are presented below and illustrated in Fig. 9.

1. An EBSD phase map is produced showing fcc austenite (γ) in blue, and bcc ferrite (δ) and martensite (α') in red in Fig. 9-a. Unindexed points (6.6%) are shown in black.
2. Only the bcc phase is shown in color as an EBSD IPF map in Fig. 9-b. Two different groups of bcc grains identified are

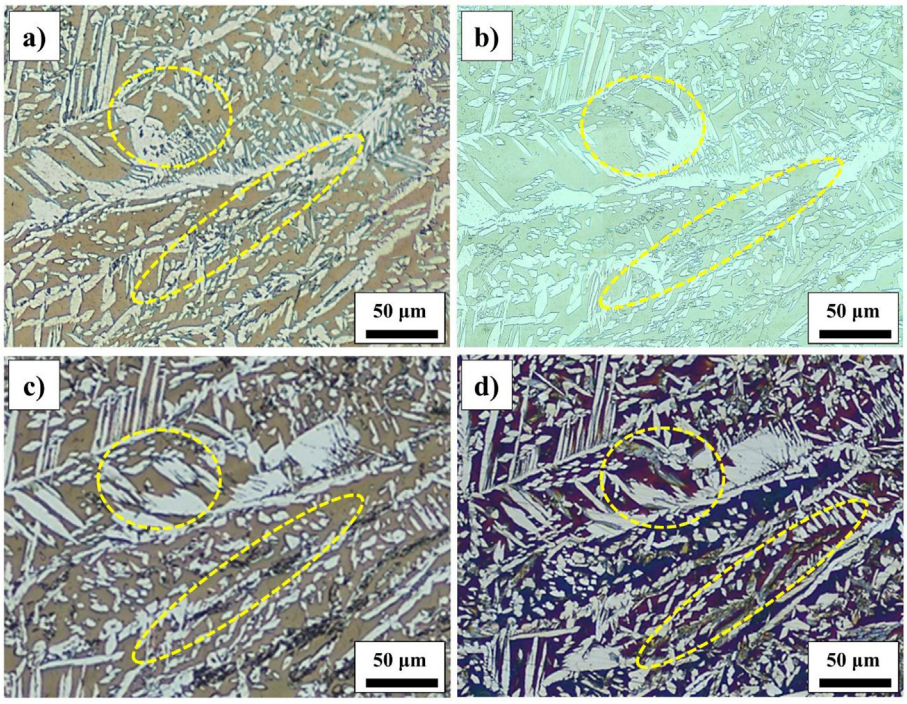

Fig. 8 – Microstructures of the WR FDX 27 TDSS after mechanical polishing followed by color etching with various Beraha etchants to identify martensite. Yellow dashed ellipses indicate regions showing the difference between the performance of various etchants. Beraha's reagent with the composition and time of 60 mL water, 30 mL HCl, and a) 0.9 g potassium bisulfite for 8–10 s; unable to distinguishing ferrite and martensite, b) 0.85 g potassium bisulfite for 10–12 s; indicating martensite boundaries without differentiating the color, c) 0.8 g potassium bisulfite for 12–15 s; over-etching of martensite, and d) 0.6 g potassium bisulfite for 10–12 s; the clear difference in colors of ferrite, austenite, and martensite.

apparent. Large grains identified as primary ferrite grains and smaller grains inside the fcc (austenite). The smaller grains are identified as martensite based on their location inside austenite and from having a different orientation compared to the large primary ferrite grains formed during solidification.

3. Based on the grain size and grain orientation, the large bcc grains (ferrite) are selected (Fig. 9-c).
4. The remaining small bcc grains are now defined as α'-martensite phase using the AZtecCrystal software (Fig. 9-d).
5. The large bcc grains are considered as ferrite and are shown in Fig. 9-e.
6. Finally, ferrite, austenite, and martensite are colored red, blue, and yellow, respectively (Fig. 9-f). The separated phases can then be quantified using the AZtecCrystal software and the result showed phase fractions of 48.7% ferrite, 31.5% austenite, and 13.2% martensite. The fraction of 6.6% unindexed points (black) remained unchanged.

4. Discussion

4.1. *Strain induced martensite*

In stainless steel, metastable austenite can transform into martensite due to applied stress or strain [27,28]. Strain-induced martensite (SIM) forms during either bulk deformation [20,29–33] or at the surface during mechanical sample preparation [11,34,35] as found in this study. Two types of martensite can be formed due to the displacement of atomic planes during deformation [36]: ε-martensite and/or α'-martensite. The formation of ε- and/or α'-martensite is influenced by the stability of austenite, governed by the austenite chemical composition, and the degree of deformation. Tian et al. [8] claimed that austenite in FDX 27 TDSS used in this study, can transform to martensite through either the $\gamma \rightarrow \varepsilon \rightarrow \alpha'$ or the $\gamma \rightarrow \alpha'$ paths. The path is determined by the degree of strain applied to the austenite. During bulk deformation, the strain and strain rate can easily be measured. Monitoring the surface strain induced by sample preparation is not practically possible, in particular when done manually. However, Rodelas et al. [11] argued that the local shear stress encountered during grinding and mechanical polishing leading to the formation of SIM is higher than during deformation of the bulk even during necking. Therefore, the formation of α'-martensite is more likely during mechanical sample preparation, which has also been reported in different studies [6,8,11].

The martensitic transformation during mechanical polishing was verified with the EBSD analysis presented in Fig. 7, and as expected DIMT resulted in the formation of α'-martensite. Although detecting small amounts of ε-martensite could be challenging with EBSD analysis [8,33], the low amount of unindexed points in EBSD analysis lent support to the absence of significant amounts of ε-martensite in the microstructure.

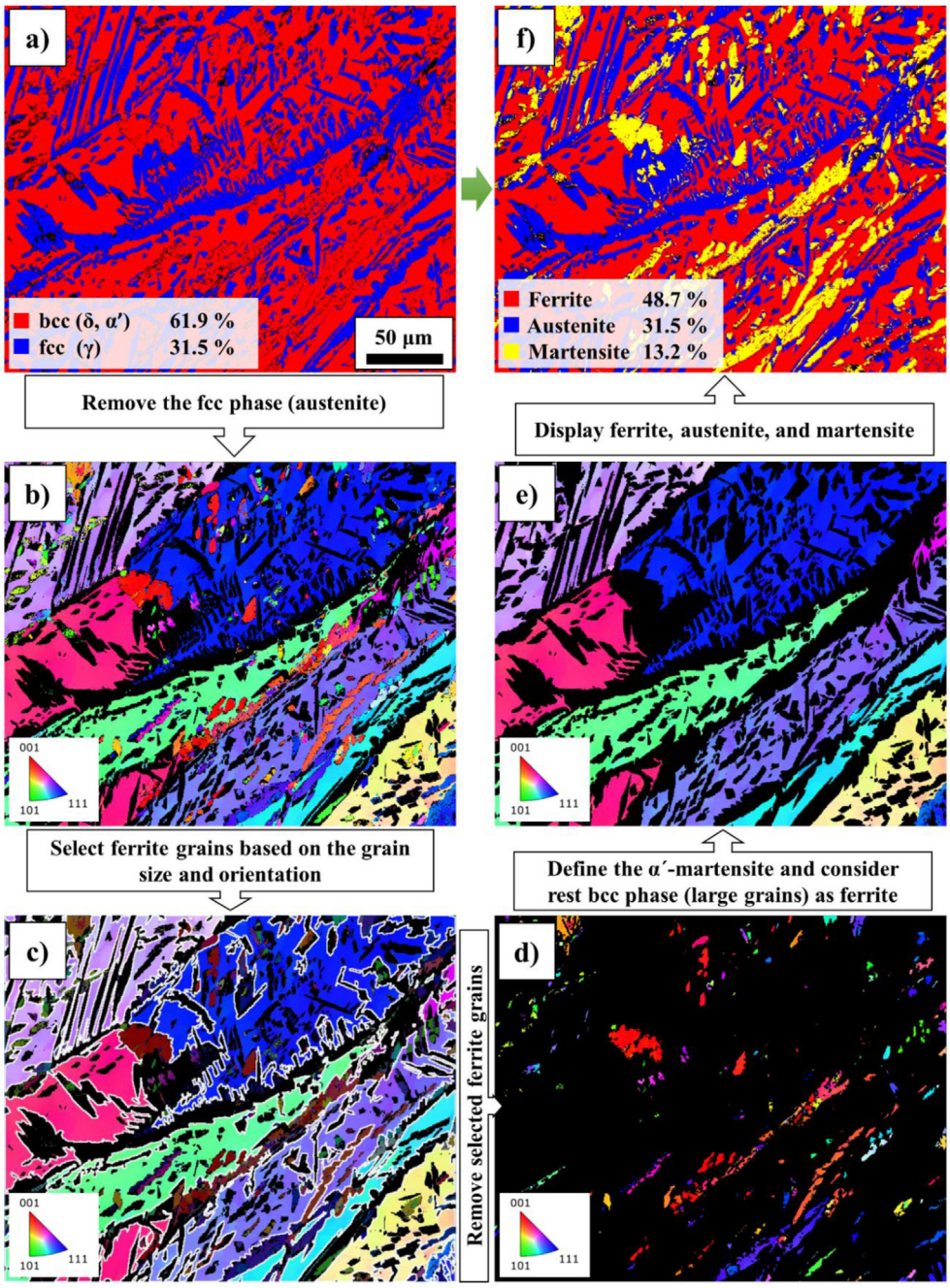

Fig. 9 – EBSD methodology for martensite identification. a) EBSD phase map with bcc (ferrite and martensite), fcc (austenite), and unindexed points (black), b) EBSD IPF map of bcc phase with big grains representative of primary solidified ferrite and small grains inside the austenite which are strain-induced martensite, c) big bcc grains (ferrite) are selected and removed, d) remaining small ferrite grains are the α'-martensite phase, e) large bcc grains are ferrite, and f) EBSD phase map containing ferrite (red), austenite (blue), and martensite (yellow) can now be shown as separate phases. The unindexed black points (6.6%) remain unchanged.

4.2. *Effects of surface preparation method*

The results clearly showed that the sample preparation method, in particular the choice of mechanical or electrolytic polishing, affects the phase fractions and the quality and accuracy of phase analysis in TDSS with both LOM and EBSD. Using electrolytic polishing instead of mechanical polishing can both prevent phase transformation during sample preparation and produce a smooth and defect-free surface suitable for EBSD analysis.

From the viewpoint of phase transformation, both LOM and EBSD analysis suggested austenite to martensite

transformation during mechanical polishing. In LOM, the microstructure of BM, as shown in Fig. 4, indicates that martensite formed in austenite grains after mechanical polishing as a consequence of the near surface plastic deformation introduced. The same behaviour of the weld metal, as seen in Fig. 5, provided compelling evidence that mechanical polishing caused the formation of SIM. Quite contrary, no martensite was seen after electrolytic polishing of neither BM nor WR, as illustrated in Figs. 4 and 5, which is in line with the fact that electrolytic polishing does not introduce any surface stresses or strains.

This result was also replicated in EBSD analysis of TDSS welds, as there was a significant difference between the bcc and fcc phase fractions after mechanical and electrolytic polishing. The lower austenite fraction after mechanical polishing confirmed the austenite to martensite transformation.

The choice of mechanical and electrolytic polishing not only affects the degree of DIMT but also has a significant effect on the quality of EBSD analysis results. In EBSD, phase analysis is based on the monitoring of the Kikuchi patterns generated by backscattered electrons [12]. In mechanical polishing, the shear stress [11] applied on the surface to remove material can affect the crystal structure close to the surface, as illustrated in Fig. 6. However, in electrolytic polishing, a chemical reaction polishes the sample, resulting in a strain-free crystal structure at the surface. Electrolytic polishing, therefore, as displayed in Fig. 6, led to a higher quality of EBSD analysis thanks to providing a more uniform and stress-free surface. This was also supported by the higher number of indexed points in the EBSD analysis after electrolytic polishing, 96.4%, compared to 93.4% after mechanical polishing.

In electrolytic polishing, perchloric acid is commonly used as a component in the electrolyte during electrolytic polishing [37–39]. In this study, however, it was replaced with another electrolyte, as introduced in experimental, for safety reasons [25,26]. During electrolytic polishing, there is a risk of pitting as a consequence of a local etching which should be prevented to achieve a uniform electrolytically polished surface [40]. Reducing the temperature is an effective way to avoid pitting during electrolytic polishing [37–39]. In this study, lowering the electrolyte temperature to around 0 °C successfully suppressed pitting. In conclusion, the current electrolytic polishing methodology was found safe and simple, which did not require special equipment.

Although electrolytic polishing is well suited for the preparation of samples for EBSD analysis, it is not recommended for LOM analysis, at least not samples for color etching. The reason is that after electrolytic polishing, a passive layer forms on the surface which suppresses a sufficient reaction of the etchant with the polished surface [40–42]. The contrast between phases, consequently, decreases significantly in comparison with samples that could be etched after mechanical polishing.

4.3. *LOM and EBSD evaluation methodologies*

In the current study, martensite formed as the consequence of DIMT during mechanical sample preparation. Phase analysis is therefore of great importance in steels such as TDSS as the content of martensite plays a vital role in determining corrosion resistance and mechanical properties. Two methodologies, therefore, based on LOM and EBSD were employed to identify and quantify martensite in the presence of ferrite and austenite.

In LOM, the relatively similar response of martensite and ferrite to the etching complicated phase fraction measurements. The accuracy and reliability of phase analysis with IA rely on defining a threshold separating phases in the image with different colors or contrast after etching. As the Beraha reagent can be modified and used with various compositions to etch and characterize phases [16,43], four different compositions of Beraha reagent and etching time were employed to maximize the contrast between ferrite, austenite, and martensite. It is illustrated in Fig. 8 that the Beraha reagent with a composition of 60 mL water, 30 mL HCl, and 0.6 g potassium bisulfite and using an etching time of 10–12 s provided an etched microstructure with distinguishable ferrite, austenite, and martensite (Fig. 8-d).

Although the implementation of this LOM methodology made the phase measurement possible, there were two main uncertainties in identification as well as the quantification of the phases. Firstly, a slight color gradient of etched martensite reduced the accuracy of quantification with IA. Secondly, the identification of whether austenite transforms into ε-martensite or α'-martensite is problematic with LOM. Based on the analysis of four images the standard deviation for ferrite was around 4–5%. This is slightly higher than found by, Hosseini et al. [16], in a study of the ferrite content welds in 2507 super DSS welds, stated that for a ferrite content of 68%, the standard deviation of IA after etching with Beraha was 2.6%.

To address the problems and limitations of LOM evaluation, a novel methodology based on the EBSD analysis was developed to identify and quantify martensite in the presence of ferrite and austenite. An EBSD phase map of the TDSS weld is shown in Fig. 9-a, in which the fcc phase is austenite, and the bcc phase is representative of both ferrite and martensite. As EBSD identifies various phases according to their crystal lattice structures, separating ferrite and austenite is straightforward owing to their bcc and fcc structures. However, both ferrite (bcc) and α'-martensite (bct) are detected as the same bcc phase with EBSD. The developed EBSD methodology, therefore, is based on DSS having a ferritic solidification mode resulting in large primary ferrite grains, that the martensite is formed from austenite and will be smaller in size and, martensite having a different grain orientation. Solidification of DSS is fully ferritic, and austenite forms in a solid-state ferrite to austenite transformation [44–49] at ferrite/ferrite grain boundaries as well as inside ferrite grains [50]. As a result, austenite grains are much smaller than ferrite grains, and hence martensite forming as a consequence of the TRIP effect inside the austenite grains in TDSS [6,8,51] will also be small. According to Fig. 9-b, the large bcc grains are therefore primary ferrite grains, and the small bcc grains, are martensite formed by DIMT. Using a bcc IPF map showing grain orientations and grain size made the separation of big bcc grains and smaller bcc grains (martensite) possible. In Fig. 9, it is presented how the implementation of this 6-stage methodology permits accurate identification and quantification of ferrite, austenite, and martensite in TDSS.

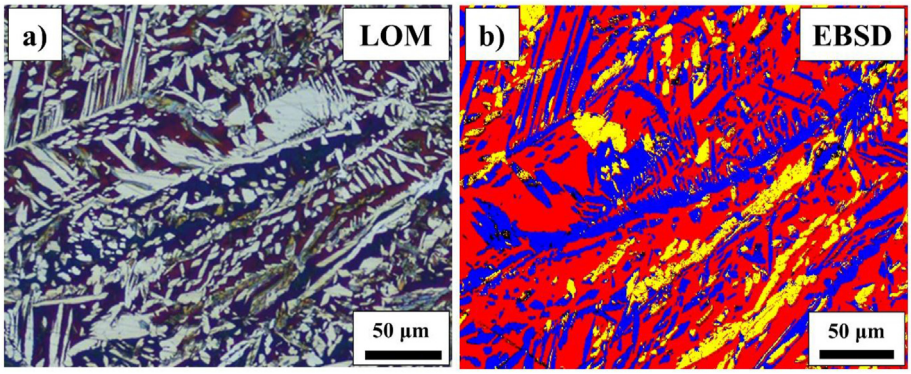

Fig. 10 – Comparison of a) LOM and b) EBSD methodologies showing martensite formation in the same regions. Martensite is colored grey in the LOM image and yellow in the EBSD image. Note that the images show the microstructure at slightly different depths as the sample was repolished after EBSD to permit color etching for LOM.

A comparison of applying the LOM and EBSD methodologies to the same region, but at slightly different depths as a consequence of repolishing, is presented in Fig. 10. The EBSD methodology is judged to have high accuracy and reliability since phases were identified in each point and there is only a low percentage of unindexed points. The LOM methodology result (16% martensite) is comparable to that from the EBSD analysis (13.2% martensite) as shown in Fig. 10 but is expected to be of less accuracy for both identification and quantification of martensite.

4.4. *Final comments*

Phase identification and quantification in multiphase steel microstructures can be approached using either classical light optical microscopy or using more recent electron microscopy techniques. Which technique is the most suitable will of course depend on the material and which phases that need to be detected. A general recommendation from the present study is that either mechanical or electrolytic polishing can be employed to prepare the surface for microstructural characterization if surface deformation is not expected to introduce phase transformations. More particularly:

- For LOM, mechanical polishing should be used if the sample is to be color etched. However, the applicability of electrolytic etching to electrolytically polished samples would be worthwhile to explore although it was out of scope for this study.
- In EBSD analysis, electrolytic polishing is preferable since it provides a smooth and strain-free surface well suited for EBSD analysis.

For steels containing austenite with low stability, only electrolytic polishing is recommended as mechanical polishing may affect phase fractions. Hence, EBSD analysis is the best alternative for phase identification and quantification. The martensite formation during mechanical sample preparation for the TDSS agreed with previous studies on steels with metastable austenite [11,34,35]. An important question for further studies is to investigate whether it would be possible to modify the mechanical polishing procedure in such a way that deformation-induced phase transformation at the surface could be avoided.

There are many stainless steels and corresponding weld metal grades that contain mixtures of at least two of the three phases martensite, ferrite, and austenite. Using color etching to distinguish phases is most probably possible for most of these. However, as illustrated in 3.2.1 (identifying martensite with LOM), this will require the adaption of the etching procedure for each specific case. The EBSD methodology is, on the other hand, more general. It is directly applicable to all DSS base metals and welds as it is based on the ferritic solidification mode of DSS, grain size and orientation. If combined with knowledge of the metallurgy of other stainless grades it should be possible to use for these as well, perhaps after some modification of the individual steps. Moreover, as fabricated components by some additive manufacturing processes, such as wire-arc and -laser direct energy deposition, have microstructures similar to weld metals, application of this methodology could also be applied for phase analysis of such materials.

This research also provides a framework for future studies to determine the general applicability of the EBSD methodology to other materials if combined with the awareness of metallurgical characteristics of multiphase material such as solidification behavior, texture, grain size, grain orientation, and morphology.

5. Conclusions

Samples from the base material and welds in a transformation-induced plasticity duplex stainless steel with metastable austenite, prepared by mechanical or electrolytic polishing, were analyzed with LOM and EBSD. Methodologies based on LOM or EBSD analysis for identification and quantification of martensite, ferrite, and austenite were developed and compared. The conclusions are as follows:

1. Mechanical polishing formed up to 26% strain-induced martensite while no martensite was introduced by electrolytic polishing.
2. Etching with the Beraha color etchant following mechanical polishing was useful for LOM studies of weld geometry and phase fraction quantification by image analysis.
3. Martensite could be identified by color etching after optimization of the etchant and etching time, but quantification was influenced by the procedure and image analysis settings.
4. Electrolytic polishing at 0 °C, using an electrolyte with the composition of 150 g citric acid, 300 g distilled water, 600 mL H_3PO_4, and 450 mL H_2SO_4 produced sufficiently stress-free, flat surfaces, free of pitting well-suited for high-quality EBSD analysis.
5. The surface characteristics of electrolytically polished samples made successful color etching difficult.
6. A novel six-steps EBSD methodology, using knowledge about the ferritic solidification of DSS and grain sizes and orientations of ferrite and martensite, was developed for the identification and quantification of martensite. The approach was shown to identify and measure the fractions of ferrite, austenite, and martensite reliably and successfully.
7. The introduced EBSD methodology is general and is, with some adaption, applicable to phase fraction analysis of many multiphase materials if combined with knowledge of the metallurgy of the specific material. It is also useful for additive manufactured materials as well as base and weld metals.

Declaration of Competing Interest

The authors declare that they have no known competing financial interests or personal relationships that could have appeared to influence the work reported in this paper.

Acknowledgments

The authors would like to thank Sten Wessman, Kjell Hurtig, and Björn Särnerblom (University West, Sweden) for their help in supplying and preparation of the samples. This study received support from the EU-project H2020-MSCA-RISE-2018 Number 823786, i-Weld, and the Swedish Agency for Economic and Regional Growth through the European Union–European Development Fund.

REFERENCES

[1] Moura AN de, Rosa Neto CA, Castro NA, Vieira EA, D'Azeredo Orlando MT. Microstructure, crystallographic texture and strain hardening behavior in hot tensile tests of UNS S32304 Lean Duplex stainless steel. J Mater Res Technol 2021;12:1065–79. https://doi.org/10.1016/j.jmrt.2021.03.023.

[2] Masoumi M, Reis FEU, Castro MO De, Béres M, Abreu HFG De. Texture evolution and phase transformation of 25Cr-6Mo-5Ni experimental duplex stainless steel during hot and cold rolling. J Mater Res Technol 2017;6:232–40. https://doi.org/10.1016/j.jmrt.2017.01.001.

[3] Morales EV, Pozo JA, Olaya L, Kassab E, Ponciano JAC, Ghavami K, et al. Remarks on the evolution and performance of the different austenite morphologies at the simulated HAZs of a 2205 duplex stainless steel. J Mater Res Technol 2019;8:3936–49. https://doi.org/10.1016/j.jmrt.2019.07.002.

[4] Potgieter JH, Olubambi PA, Cornish L, Machio CN, Sherif ESM. Influence of nickel additions on the corrosion behaviour of low nitrogen 22% Cr series duplex stainless steels. Corrosion Sci 2008;50:2572–9. https://doi.org/10.1016/j.corsci.2008.05.023.

[5] Lai JKL, Wong KW, Li DJ. Effect of solution treatment on the transformation behaviour of cold-rolled duplex stainless steels. Mater Sci Eng, A 1995;203:356–64. https://doi.org/10.1016/0921-5093(95)09863-1.

[6] Choi JY, Park KT. Secondary austenite formation during aging of hot-rolled plate of a TRIP-aided Mo-free lean duplex stainless steel. Met Mater Int 2020;2. https://doi.org/10.1007/s12540-020-00689-7.

[7] Herrera C, Ponge D, Raabe D. Design of a novel Mn-based 1 GPa duplex stainless TRIP steel with 60% ductility by a reduction of austenite stability. Acta Mater 2011;59:4653–64. https://doi.org/10.1016/j.actamat.2011.04.011.

[8] Tian Y, Lin S, Ko JYP, Lienert U, Borgenstam A, Hedström P. Micromechanics and microstructure evolution during in situ uniaxial tensile loading of TRIP-assisted duplex stainless steels. Mater Sci Eng, A 2018;734:281–90. https://doi.org/10.1016/j.msea.2018.07.040.

[9] Choi JY, Ji JH, Hwang SW, Park KT. Effects of nitrogen content on TRIP of Fe-20Cr-5Mn-xN duplex stainless steel. Mater Sci Eng, A 2012;534:673–80. https://doi.org/10.1016/j.msea.2011.12.025.

[10] Jiang S yong, Wang Y, Xing X dong, Zhang Y qiu. Stress-induced martensite phase transformation of FeMnSiCrNi shape memory alloy subjected to mechanical vibrating polishing. Trans Nonferrous Met Soc China (English Ed 2020;30:1582–93. https://doi.org/10.1016/S1003-6326(20)65321-3.

[11] Rodelas JM, Maguire MC, Michael JR. martensite formation in the metallographic preparation of austenitic stainless steel welds. Microsc Microanal 2013;19:1748–9. https://doi.org/10.1017/s1431927613010738.

[12] Pinto LA, Pérez Escobar D, Santos OSH, Lopes NIA, Carneiro JRG, Ribeiro-Andrade R. Influence of surface preparation method on retained austenite quantification. Mater Today Commun 2020;24. https://doi.org/10.1016/j.mtcomm.2020.101226.

[13] Kang JY, Kim DH, Baik S Il, Ahn TH, Kim YW, Han HN, et al. Phase analysis of steels by grain-averaged EBSD functions. ISIJ Int 2011;51:130–6. https://doi.org/10.2355/isijinternational.51.130.

[14] Dobras D, Rutkowska-Gorczyca M. Application of color etching to study the microstructure of TRIP steel after laser remelting. Weld Technol Rev 2018;90:14–9. https://doi.org/10.26628/wtr.v90i12.984.

[15] Celada-Casero C, Kooiker H, Groen M, Post J, San-Martin D. In-situ investigation of strain-induced martensitic transformation kinetics in an austenitic stainless steel by inductive measurements. Metals (Basel) 2017;7. https://doi.org/10.3390/met7070271.

[16] Hosseini V, Hurtig K, Eyzop D, Östberg A, Janiak P, Karlsson L, et al. Ferrite content measurement in super duplex stainless steel welds. Weld World 2019;63:551–63. https://doi.org/10.1007/s40194-018-00681-1.

[17] Bassani P, Breda M, Brunelli K, Mészáros I, Passaretti F, Zanellato M, et al. Characterization of a cold-rolled 2101 lean duplex stainless steel. Microsc Microanal 2013;19:988–95. https://doi.org/10.1017/S1431927613001426.
[18] De AK, Murdock DC, Mataya MC, Speer JG, Matlock DK. Quantitative measurement of deformation-induced martensite in 304 stainless steel by X-ray diffraction. Scripta Mater 2004;50:1445–9. https://doi.org/10.1016/j.scriptamat.2004.03.011.
[19] Mangonon P, Thomas G. Structure and properties of thermal-mechanically treated 304 stainless steel. OR Trans 1970;1:1587–94.
[20] Solomon N, Solomon I. Deformation induced martensite in AISI 316 stainless steel. Rev Metal 2010;46:121–8. https://doi.org/10.3989/revmetalm.0920.
[21] Filippone R, Root J, Jacques P, Yue S. The influence of martensite on line broadening in neutron diffraction spectra of a DP steel. ISIJ Int 2002;42:304–9. https://doi.org/10.2355/isijinternational.42.304.
[22] Kaňa V, Pernica V, Zadera A, Krutiš V. Comparison of methods for determining the ferrite content in duplex cast steels. Arch Foundry Eng 2019;19:85–90. https://doi.org/10.24425/afe.2019.127121.
[23] Talonen J, Aspegren P, Hänninen H. Comparison of different methods for measuring strain induced α′-martensite content in austenitic steels. Mater Sci Technol 2004;20:1506–12. https://doi.org/10.1179/026708304X4367.
[24] Baghdadchi A, Hosseini VA, Hurtig K, Karlsson L. Promoting austenite formation in laser welding of duplex stainless steel—impact of shielding gas and laser reheating. Weld World 2020. https://doi.org/10.1007/s40194-020-01026-7.
[25] Pearson GS. Perchloric acid. In: Adv. Inorg. Chem. Radiochem., vol. 8. Elsevier; 1966. p. 177–224.
[26] Schilt AA, McBride L, Long JR. Perchloric acid and perchlorates. Columbus, OH: GF Smith Chemical Company; 1979.
[27] Olson GB, Cohen M. A mechanism for the strain-induced martensitic transformations. J Less-Common Met 1972;28:107–18.
[28] Olson GB, Cohen M. A general mechanism of martensitic nucleation: Part II. FCC→BCC and other martensitic transformations. Metall Trans A 1976;7:1905–14. https://doi.org/10.1007/BF02654988.
[29] Talonen J, Hänninen H. Formation of shear bands and strain-induced martensite during plastic deformation of metastable austenitic stainless steels. Acta Mater 2007;55:6108–18. https://doi.org/10.1016/j.actamat.2007.07.015.
[30] Weiß A, Gutte H, Scheller PR. Deformation induced martensite formation and its effect on Transformation Induced Plasticity (TRIP). Steel Res Int 2006;77:727–32. https://doi.org/10.1002/srin.200606454.
[31] Das A, Sivaprasad S, Ghosh M, Chakraborti PC, Tarafder S. Morphologies and characteristics of deformation induced martensite during tensile deformation of 304 LN stainless steel. Mater Sci Eng, A 2008;486:283–6.
[32] Ryoo DY, Kang N, Kang CY. Effect of Ni content on the tensile properties and strain-induced martensite transformation for 304 stainless steel. Mater Sci Eng, A 2011;528:2277–81. https://doi.org/10.1016/j.msea.2010.12.022.
[33] Lü Y, Hutchinson B, Molodov DA, Gottstein G. Effect of deformation and annealing on the formation and reversion of ε-martensite in an Fe-Mn-C alloy. Acta Mater 2010;58:3079–90. https://doi.org/10.1016/j.actamat.2010.01.045.
[34] Juuti T, Uusikallio S, Kaijalainen A, Heinonen E, Tun NT, Porter D. The effect of sample preparation on the microstructure of austenitic-ferritic stainless steel. Mater Sci Forum 2017;879:873–8. https://doi.org/10.4028/www.scientific.net/MSF.879.873.
[35] Knipling KE, Rowenhorst DJ, Fonda RW, Spanos G. Effects of focused ion beam milling on austenite stability in ferrous alloys. Mater Char 2010;61:1–6. https://doi.org/10.1016/j.matchar.2009.09.013.
[36] Tavares SSM, Pardal JM, da Silva MJG, Abreu HFG, da Silva MR. Deformation induced martensitic transformation in a 201 modified austenitic stainless steel. Mater Char 2009;60:907–11. https://doi.org/10.1016/j.matchar.2009.02.001.
[37] Haghdadi N, Cizek P, Beladi H, Hodgson PD. The austenite microstructure evolution in a duplex stainless steel subjected to hot deformation. Philos Mag A 2017;97:1209–37. https://doi.org/10.1080/14786435.2017.1293860.
[38] Cizek P. The microstructure evolution and softening processes during high-temperature deformation of a 21Cr-10Ni-3Mo duplex stainless steel. Acta Mater 2016;106:129–43. https://doi.org/10.1016/j.actamat.2016.01.012.
[39] Gabe DR. Electropolishing of mild steel in phosphoric and perchloric acid containing electrolytes. Corrosion Sci 1973;13:175–85.
[40] Mohan S, Kanagaraj D, Sindhuja R, Vijayalakshmi S, Renganathan NG. Electropolishing of stainless steel - a review. Trans Inst Met Finish 2001;79:140–2. https://doi.org/10.1080/00202967.2001.11871382.
[41] Rokosz K, Hryniewicz T, Solecki G. Comparative corrosion studies of 2205 duplex steel after electropolishing and passivation in Ringer's solution. World Sci News 2018;95:167–81.
[42] Vignal V, Krawiec H, Le Manchet S. Influence of surface preparation and microstructure on the passivity and corrosion behaviour of duplex stainless steels. J Solid State Electrochem 2014;18:2947–54. https://doi.org/10.1007/s10008-013-2364-0.
[43] Britz D, Webel J, Schneider AS, Mücklich F. Identifying and quantifying microstructures in low-alloyed steels: a correlative approach. Metall Ital 2017;109:5–10.
[44] Lippold JC, Kotecki DJ, Sant S. Welding metallurgy and weldability of stainless steels. MRS Bull Res Soc 2006;31:58.
[45] Ogawa T, Koseki T. Effect of composition profiles on metallurgy and corrosion behavior of duplex stainless steel weld metals. Weld J 1989;68:181.
[46] Varol I, Baeslack WA, Lippold JC. Characterization of weld solidification cracking in a duplex stainless steel. Mater Char 1997;39:555–73. https://doi.org/10.1016/s1044-5803(97)00144-7.
[47] Zhu C, Zeng J, Wang W, Chang S, Lu C. Mechanism of $\delta \rightarrow \delta + \gamma$ phase transformation and hardening behavior of duplex stainless steel via sub-rapid solidification process. Mater Char 2020;170:110679. https://doi.org/10.1016/j.matchar.2020.110679.
[48] Mirakhorli F, Malek Ghaini F, Torkamany MJ. Development of weld metal microstructures in pulsed laser welding of duplex stainless steel. J Mater Eng Perform 2012;21:2173–6. https://doi.org/10.1007/s11665-012-0141-3.
[49] Jiang ZL, Chen XY, Huang H, Liu XY. Grain refinement of Cr25Ni5Mo1.5 duplex stainless steel by heat treatment. Mater Sci Eng, A 2003;363:263–7. https://doi.org/10.1016/S0921-5093(03)00647-6.
[50] Karlsson L. Welding duplex stainless steels - a review of current recommendations. Weld World 2012;56:65–76. https://doi.org/10.5937/zzk1802065k.
[51] Tian Y, Gorbatov OI, Borgenstam A, Ruban AV, Hedström P. Deformation microstructure and deformation-induced martensite in austenitic Fe-Cr-Ni alloys depending on stacking fault energy. Metall Mater Trans A Phys Metall Mater Sci 2017;48:1–7. https://doi.org/10.1007/s11661-016-3839-2.